EXPERIMENTAL BEHAVIOR OF CHROMIUM-BASED COATINGS

J. KREJČÍ, M. ŠEVEČEK
CTU in Prague, Faculty of Nuclear Sciences and Physical Engineering, V Holešovičkách 2, 18000 Praha 8

J. KABÁTOVÁ, F. MANOCH, J. KOČÍ
UJP PRAHA a.s., Nad Kamínkou 1345, 156 10 Praha - Zbraslav

L. CVRČEK, J. MÁLEK, S. KRUM
CTU in Prague, Faculty of Mechanical Engineering, Karlovo náměstí 293/13, 12000 Praha 2

P. ŠUTTA
University of West Bohemia, New Technologies – Research Centre, Teslova 9a, 30100 Plzeň

P. BUBLÍKOVÁ, P. HALODOVÁ, H. K. NAMBURI
Research Centre Řež, Hlavní 130, 25068 Husinec – Řež

ABSTRACT

Accident Tolerant Fuels have been widely studied since the Fukushima accident in 2011. Deposition of protective coatings on nuclear fuel claddings has been considered as a near-term concept that will reduce the high-temperature oxidation rate of zirconium-based alloys and enhance accident tolerance of reactor cores by providing additional coping time. This study is focused on low-temperature oxidation and LOCA experimental behavior of Zr-1%Nb cladding alloys coated with Cr and CrN based layers by PVD technique. Coated and reference uncoated samples of Zr-1%Nb alloy were tested in several experiments. The presented results include standard corrosion tests at 360°C in WWER water chemistry, burst tests and mainly single and double-sided high-temperature steam oxidation between 1000 and 1400°C. Coated and reference samples were characterized pre- and post-testing using mechanical testing (microhardness, ring compression test), TEA analysis (hydrogen, oxygen measurements), optical microscopy, scanning electron microscopy (EDS, WDS, EBSD) and other techniques including X-ray diffraction.

1 Introduction

The research of Accident Tolerant Fuels (ATF) accelerated due to the Fukushima accident in 2011 and various concepts have been developed around the world. The ultimate objective of the ATF materials is to provide additional coping time in case of an accident of a Light Water Reactor (LWR). There are different concepts being developed around the world from modifications of current technologies to introduction of revolutionary materials. Generally, new fuels, cladding materials or non-fuel components considered as ATFs have been proposed [1]–[3]. The near-term options for cladding materials include mainly multi-layer claddings where traditional Zr-based alloys serve as a substrate and different layers are applied as a protective coating on the substrate [4]–[6]. The Zr-based substrate still acts as the main structural component and the coatings applied on its surface can provide different functions such as corrosion or wear resistance, diffusion barrier etc.

This paper presents results on testing of cladding with enhanced accident tolerance with a focus on WWER reactors. The multicomponent concept is based on the Zr-1%Nb alloy with different Cr-based layers deposited on the substrate alloy. Its focus is on WWER reactors but the results of behavior in accidental conditions are applicable also for other LWRs [7]. The high-temperature behavior of cladding materials coated with pure chromium was widely studied by [4], [8]–[12] and others, but the behavior varies based on the deposition techniques, deposition parameters and thickness used. Chromium nitride coated cladding materials are also considered as a potential ATF candidate but the published results in accidental behavior are in comparison with chromium coated materials limited [13]–[17]. Two

other Cr-based coatings were proposed for testing that have not been studied to date – substoichiometric CrN and multicomponent CrN+Cr coatings. These two materials were proposed as promising coatings that can reduce or avoid negative effects entailed to metallic Cr and ceramic CrN (namely – Cr+Zr eutectic formation; Cr enhanced embrittlement of Zr; CrN cracking at high temperature due to phase changes).
Presented study is focused on corrosion behavior at normal operating conditions, design basis accident conditions (loss of coolant accident (LOCA), high-temperature oxidation up to 1200°C) and on fuel cladding performance in beyond design extension conditions.

2 Methods

2.1 Materials and Coatings

The tests presented in this paper were performed using the Zr-1%Nb alloy (E110), which is used mainly in the WWER reactors as the fuel cladding. The chemical composition is shown in Table 1. Tested non-irradiated segments had the outer diameter of 9.1 mm and length of 15 - 30 mm (double-sided oxidation) and 30 – 75 mm (single-sided oxidation). The thickness of the tube's wall is about 0.6 mm.

wt. %	Nb	Fe	O	Zr
E110	1.01	0.05	0.071	balance

Table 1. The chemical composition of the Zr-1%Nb cladding material that was used as the substrate.

Coatings were deposited on outer surfaces of Zr tubes by magnetron sputtering from Cr (99.6 %) targets in the Hauzer Flexicoat 850 industrial system. Pure metallic chromium coatings were prepared in the argon atmosphere and CrN coatings in a gas mixture of argon and nitrogen at the deposition temperature of 250°C for each coating. As the coatings to be tested chromium, chromium nitride (CrN), sub-stochiometric CrN (Cr 90 wt.% and N 10 wt.%) and two variants of multi-layer coatings ("thin" CrN+Cr and "thick" CrN+Cr) were selected. Before deposition, the tubes were ultrasonically cleaned in acetone, ethanol, DI water and dried with a blower. The tubes were placed into the vacuum chamber on rotating holders in the Flexicoat system where they were cleaned by ion etching in the argon plasma. This process removes the thin Zr-oxide and other impurities thus improving adhesion of the coating. The deposition parameters varied depending on the particular coating. A thin metallic layer was deposited on the substrate first when depositing ceramic coatings to improve adhesion. The thickness of the as-deposited coatings was measured by an optical microscope and LUCIA G image analyzer and results are summarized in Table 2.

Coating	Cr1	Cr2	CrN	$Cr_{90}N_{10}$	CrN+Cr1	CrN+Cr2
Thickness (μm)	10.6 ± 0.6	30.4 ± 0.7	12.8 ± 0.3	18 ± 0.6	3.2+19.4	12.8+24.8

Table 2. Measured thicknesses of applied coatings.

2.2 Autoclave Oxidation

Coated tubular specimens for single-sided oxidation were cleaned, degreased, and then weighted. Afterward, the specimens were placed into a static autoclave in standard WWER environment (B: 1050 ppm, K: 15.9 ppm, Li: 1 ppm) at 360°C and 197 bar. After each time period (21 days), samples were weighted. Several samples were cut, hydrogen content was measured and cross-section analysis using an optical microscope was performed.

2.3 High-temperature Oxidation

Coated tubular segments were cleaned, degreased, and then weighted. The specimens were then exposed for variable time intervals to high-temperature steam at low pressure (0.1 MPa). The test was performed in a resistance furnace at a constant temperature. The oxidation was double-sided or single-sided. In case of single-sided oxidation, end caps were welded onto the coated tubular samples after the deposition by TIG method. The temperature was measured by a thermocouple placed next to sample surface. At the end of the test, the sample was quenched in ice water. Schematic representation of apparatus is shown in Fig. 1.

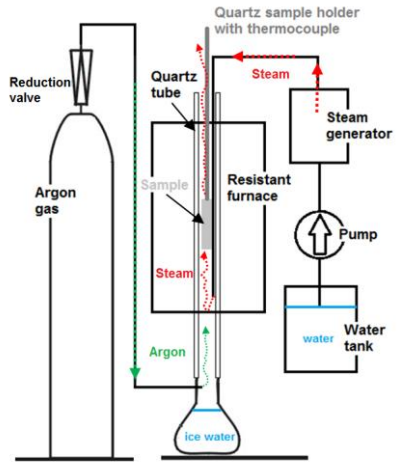

Fig. 1: Schematic representation of the apparatus used in high-temperature steam oxidation experiments.

2.4 Material Characterization

The samples were characterized in as-coated state and after the testing. After the test, the specimens were first dried out and weighted. Later, the segments of a fuel cladding were visually evaluated and cut into several rings for further investigation. Following tests were performed:

- Metallographic analysis
- Microhardness
- EBSD
- X-ray Diffraction
- SEM
- EDS, WDS
- Hydrogen, oxygen measurement
- Ring compression test

The metallographic cross sections were prepared using the standard polishing procedure and metallographic evaluation followed. The thickness of the chromium oxide layer, ZrO_2 layer and the α-Zr(O) layer (including the grains extended towards the β-phase region) was measured in several directions at both inner and outer cladding edges. The optical microscope NIKON Elipse MA200 and LUCIA G image analyzer were used for the metallographic analysis.

The metallographic cross sections were used for microhardness measurements in several positions of the tube wall. For single-sided oxidation, 3 rows with 10 measurements were done (under the coating, in the middle of the wall, close to the inner side) and for double-sided oxidation, 2 rows with 10 measurements in the middle of the wall were performed.

EBSD map was measured for coatings in the as-received state using the JEOL LSM 7600F microscope equipped with Nordly's II EBSD detector. Obtained data were processed in "hkl Channel 5" software package.

XRD instrument X'Pert equipped by the semi-conductive PIXcel detector and a radiance furnace was used for XRD analysis of sample surface in as-received state and during a high-temperature transient.

Scanning Electron Microscopes (JEOL: JSM 5510 LV and Tescan Lyra3 GMU) were used for Energy Disperse X-ray Spectroscopy (EDS). Scanning Electron microscope Tescan Lyra3 GMU with Field Emission Gun was used for Wavelength Dispersive X-ray Spectroscopy (WDS). The chemical composition was analyzed by automated chemical profiles using Oxford INCAWave system

Two 7 mm long rings were cut from the specimens after single-sided oxidation tests and ring-compression-tests (RCT) at 135°C were performed using the INSTRON 1185 machine.

Other parts of the samples intended for bulk hydrogen content measurements using the Analyzer G8 GALILEO (Bruker), which works on the inert gas fusion principle. Several rings

from different parts of the sample wall were prepared on a lathe machine. First, the coating was removed, afterward, the inner or outer side of the wall was machined to prepare the required ring for analysis, as can be seen in Fig. 2. Using this methodology, it was possible to analyze bulk oxygen content in the inner and outer part of the wall. Bulk oxygen content was measured using the Analyzer G8 GALILEO.

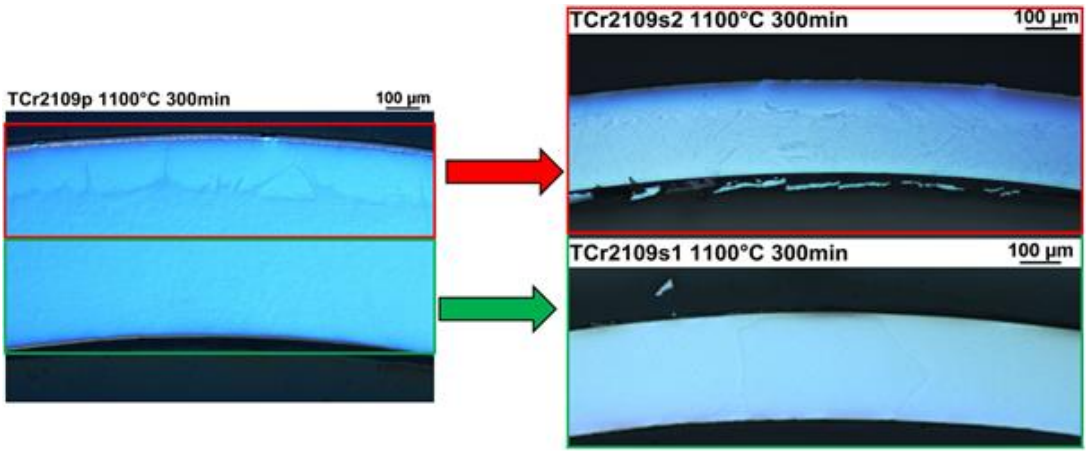

Fig. 2: Sample preparation for bulk oxygen content measurements. Specimen after high-temperature oxidation (left) and two rings (the outer part after removing the coating and inner part) after machining

3 Results

3.1 As-received Coatings

Several specimens were used for the EBSD analysis after the PVD deposition of the coatings. Figure 3 shows the comparison of EBSD analysis of pure Cr coatings labeled Cr1 and Cr2. The 10 µm thick coating (Cr1) showed a higher level of orientation in comparison with the thicker coating Cr2. The main direction of orientation is 001 in perpendicular Y-direction to the sample surface.

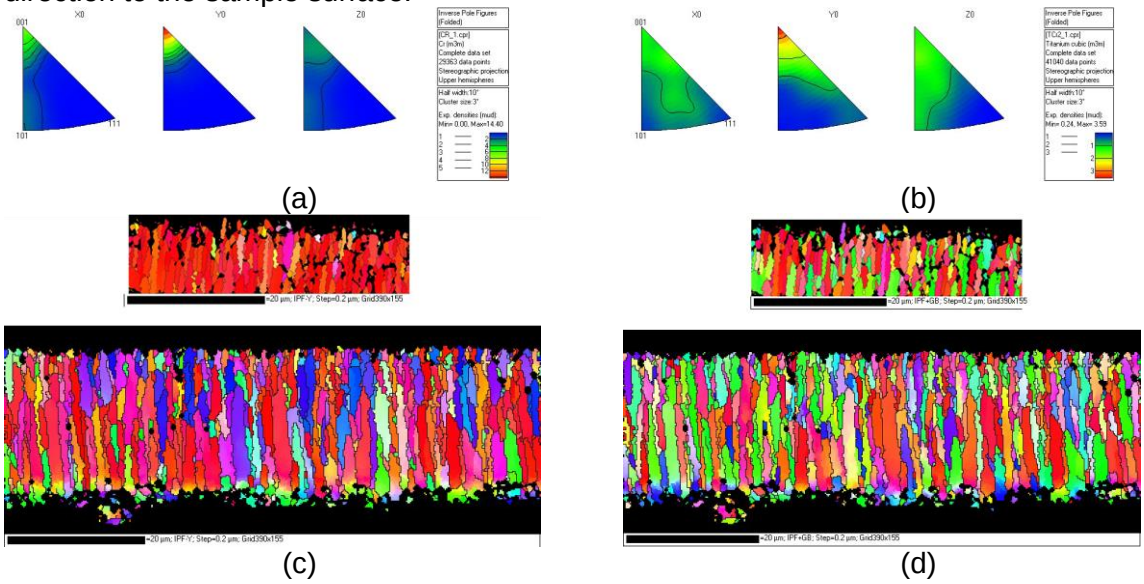

Fig. 3: EBSD results: (a) grain orientation for Cr1 (10 µm) coating, (b) grain orientation for Cr2 (30 µm) coating, (c) EBSD map for perpendicular Y-direction (Cr1 up, Cr2 down), (d) EBSD map for parallel X,Z-direction (Cr1 up, Cr2 down).

This very strong Cr-coating orientation shown in Figure 3 was confirmed using the XRD instrument X'Pert equipped with semi-conductive PIXcel detector (scanned sample surface 20 mm^2). From the diffraction patterns shown in Figure 4, the high degree of crystallinity of Cr-coating is obvious. Very narrow peaks suggest a bigger size of crystalline regions in case

of metallic Cr (black line). In contrast, the structure of stoichiometric CrN coating was more amorphous as shown by the diffraction pattern (red line). These results were confirmed by the fracture analysis of both coatings (pure Cr, stoichiometric CrN) shown in Figure 5. The structure of applied Cr and CrN coatings has columnar growth according to Thornton structure zone model typical for magnetron sputtering method.

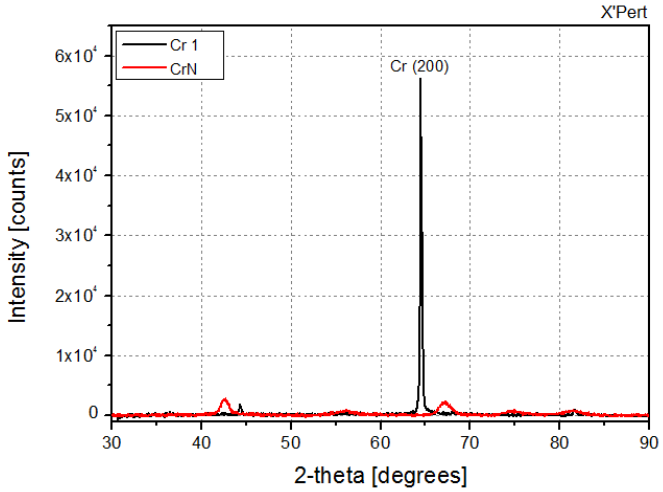

Fig. 4: XRD diffractograms for Cr1 and CrN coatings.

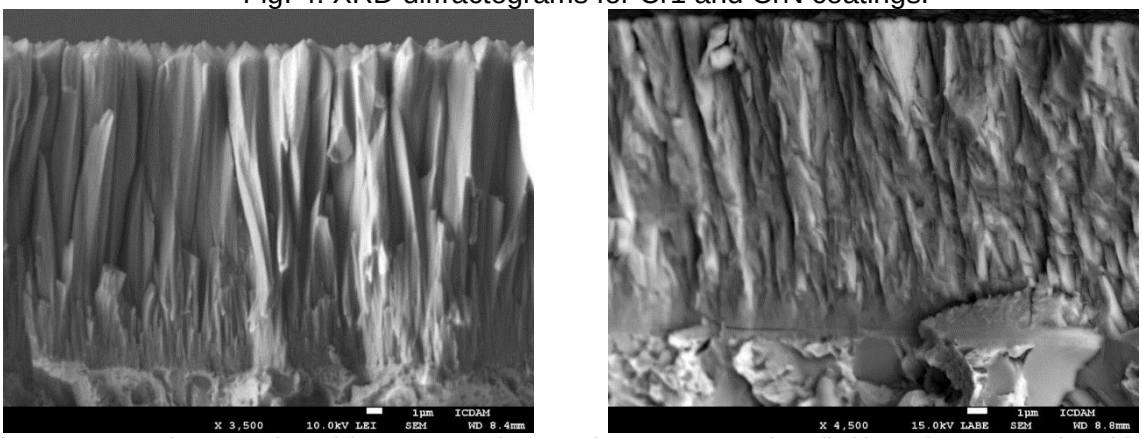

Fig. 5: SEM micrographs of fracture surfaces of pure Cr-coating (left) and CrN-coating (right).

3.2 XRD-analysis after High-temperature Transient

The X'Pert instrument equipped with radiance furnace was used for measurements of coating transformations during a high-temperature transient. Measurements were done at temperatures 25, 250, 500, 700, 900, 1100, 30°C. The length of the time step for each temperature was about 250 sec. Following diffractograms show the comparison of Cr1 and CrN coatings before and after the temperature transient. The experiment was performed in a high vacuum environment, however, the Cr_2O_3 formation was observed in both cases at temperatures above 900°C.

For both coatings, the surface of the sample was oxidized (Cr_2O_3 formation) during the temperature transient. In case of Cr1 sample, Cr (200) stays under the Cr-oxide layer. The peak at the value 35° 2-theta is slightly discussable. It corresponds to both Cr_2Zr and Zr(002). Zr(002) shows better agreement with the database. On the other hand, this diffraction line was not detected for CrN-coating where no Cr-Zr interaction was observed. Diffractogram for CrN-coating shows also the formation of Cr_2O_3 and nitrogen diffusion from the coating. Additionally, Cr(110) was crystallized. Remaining nitrogen atoms in the coating formed Cr_2N(110). It can be concluded based on the narrow peaks measured after the temperature transient, that the degree of crystallinity is much higher than before transient for CrN coating.

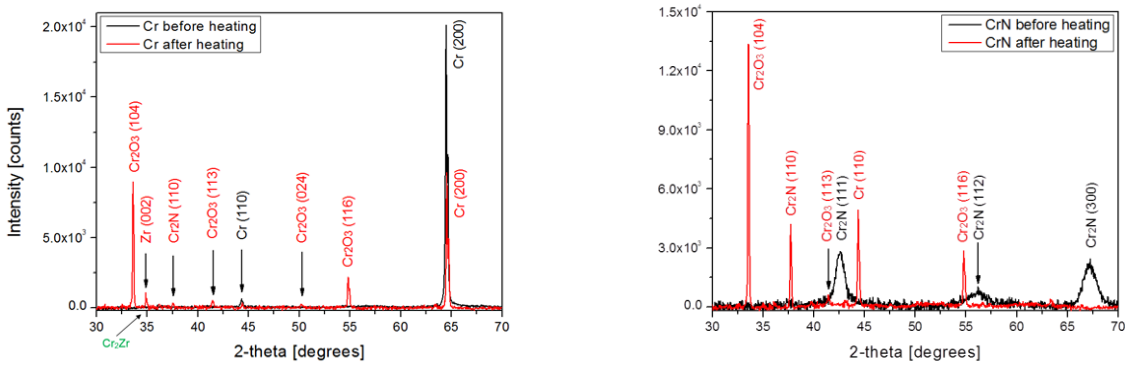

Fig. 6: XRD diffractograms of Cr1 (left) and CrN (right) coatings before and after temperature transient.

3.3 Autoclave Corrosion Test in WWER Conditions

The autoclave single-side corrosion test was performed for 5 Cr2-coated and 15 uncoated Zr1Nb samples. No coating spallation within 210 days of exposition was observed from cladding surface, except the part of the sample, where TIG welding was done to seal the sample with an inner pressure. This welding procedure was performed after the coating was deposited on the tubular sample. Photo of the sample with the spalling layer is shown in Figure 7.

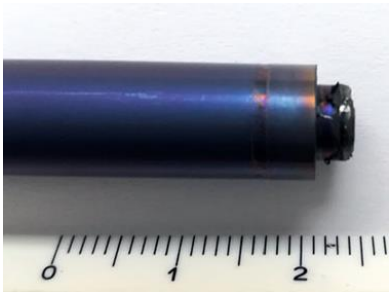

Fig. 7: Detail of sample with spalling coating after TIG welding.

Weight gain measurements were performed for each period (21 days) of exposition. For cross-section metallography and hydrogen content analysis, two uncoated samples (63 and 148 days) and two Cr-coated samples (105 and 210 days) were used. The results are summarized in Figure 8. Weight gain for Cr-coated samples is very low and after 100 days is practically constant. Hydrogen content is slightly lower than for uncoated sample (16 ppm after 210 days). Generally, the absolute values of weight gains for all samples are very low when E110 alloy is used in WWER conditions. Much higher differences in corrosion resistance can be expected e.g. for coated and uncoated Zircaloy alloys in different chemistries as shown in [5], [13].

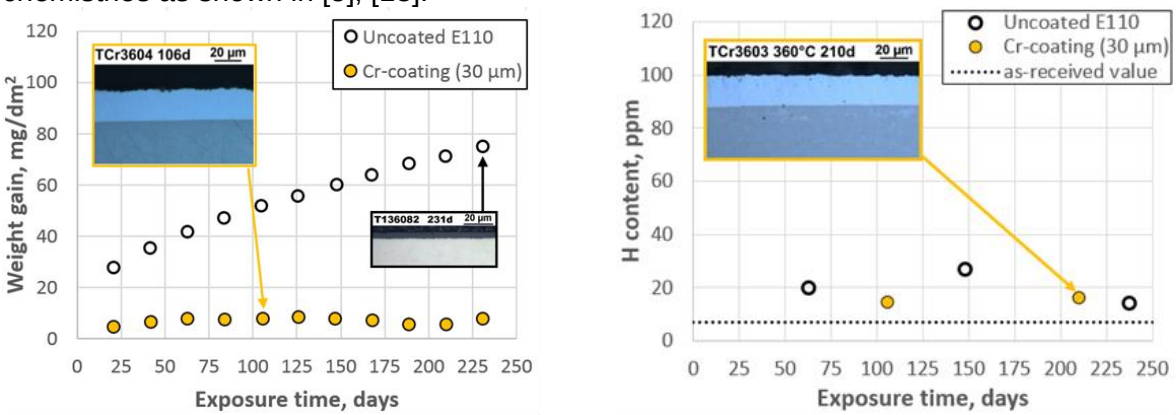

Fig. 8: Results of corrosion experiment with coated and uncoated samples in WWER environment at 360°C and 197 bar, weight gain (left) and hydrogen content (right).

The very strong protective behavior of Cr2-coating was confirmed also by in the in-situ corrosion experiment. The evaluated charge transfer resistance (corresponding to the reciprocal value of corrosion rate) for Cr-coated samples was 10x higher [18].

3.4 High-temperature Oxidation of Cr-coated Samples

The visual evaluation showed very compact black or black-green surface for all samples after the test. No nodular corrosion or cladding spallation was observed. Very low weight gain was observed for most of the samples.

After the weight gain evaluation, the single-sided oxidized specimens were cut and ring compression tests at 135°C were performed. The results are shown in plots in Figure 8. From the comparison of uncoated (blank marks) and coated (filled marks) samples, the protective behavior of Cr-coating is obvious. The plot shows residual ductility in relation with the Cathcart-Pawel ECR calculation (Fig. 9 left) [19]. Based on this plot, applied 30 μm Cr-coating enhances the accident tolerance above current DBA limits. For the samples oxidized at 1200°C/1hour and for 1100°C/5hours, and 1000 °C/48hours no DBT was observed.

On the other hand, comparison of residual ductility of coated and uncoated samples in relation with experimental ECR (Fig. 9 right) shows that methodology based on weight gain evaluation is not applicable: for very low weight gains (3 – 5 ECR%) the samples are brittle which is in conflict with current safety criteria [20]–[22]. The hydrogen content was analyzed by the TEA method and all samples show very low values – up to 120 ppm. Therefore, it was deducted, that early DBT transition is not caused by increased hydrogen content.

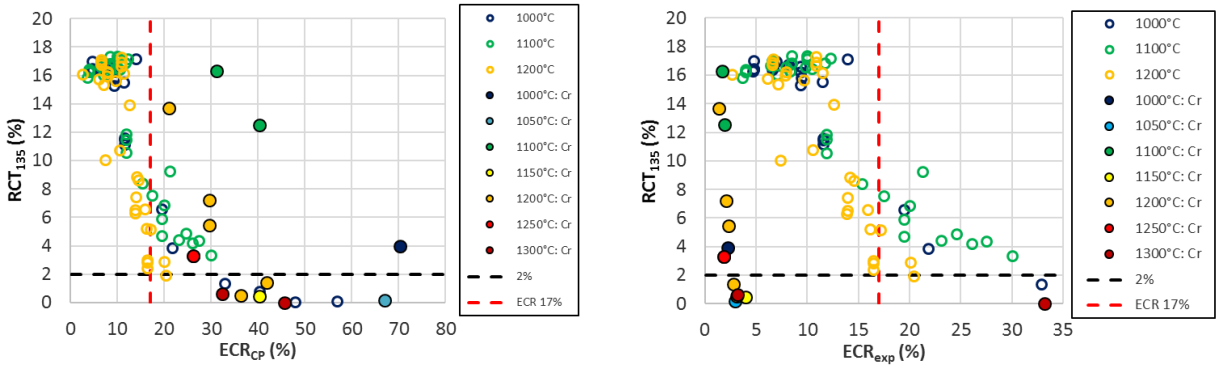

Fig. 9: Results of RCT residual ductility at 135 °C in relation with ECR-CP (left) and experimental ECR (right). Comparison of Cr-coated and uncoated specimens.

Microstructure evaluation using the optical microscope showed the different character of the Cr-coated specimen in comparison with the typical microstructure of oxidized uncoated Zr-alloys. No α-Zr(O) grains were observed for Cr-coated material, as is shown in Figure 10. Chemical composition (Cr, Zr) in the wall was analyzed using the EDS (not shown here) and WDS. For three variants of tested coatings (pure Cr, substoichiometric $Cr_{90}N_{10}$, multilayer CrN+Cr), Cr-diffusion into substrate was observed. Only the CrN-coated specimens formed ZrN layer under the coating during the high-temperature transient which reduced Cr-diffusion into the substrate. For these samples, typical α-Zr(O) grains with incursion towards prior β-Zr were observed.

Chemical composition (Cr, Zr, O, Nb elements) was analyzed using the WDS profiles up to 220 μm. The distance between analytical points was 1 μm. The profile of the average weight content for each element measured is plotted in Fig. 11 with the micrograph showed in the backscatter electron mode.

Machining procedure described in Fig. 2 was used for ring-sample preparation. No differences in bulk oxygen content for outer and inner rings were observed. However, it was found that the very high value of diffusion coefficient caused uniform oxygen distribution in prior β-Zr. Measured values of oxygen content in relation with RCT residual ductility at 135°C are shown in Fig. 12 (left). The results show good agreement with DBT for uncoated E110 [23] and M5 [24] alloys. DBT was observed for samples with oxygen content above 0.4 wt.%.

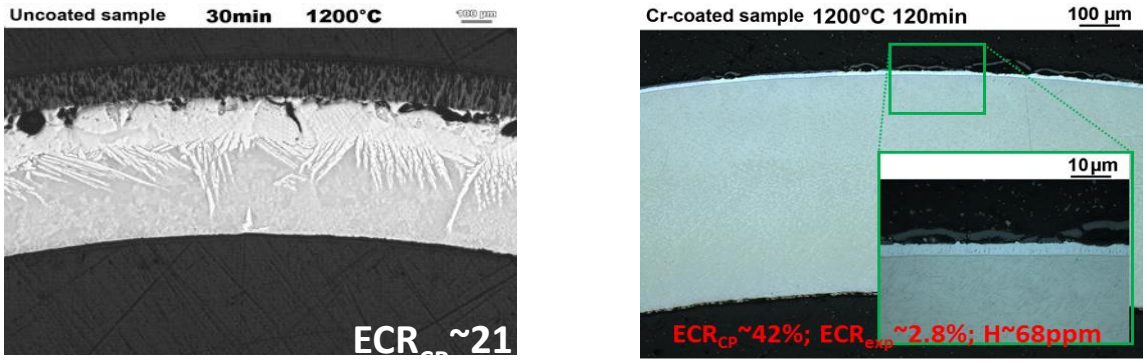

Fig. 10: Microstructures of uncoated (left) and Cr-coated (right) E110 samples after high-temperature steam oxidation at 1200 °C.

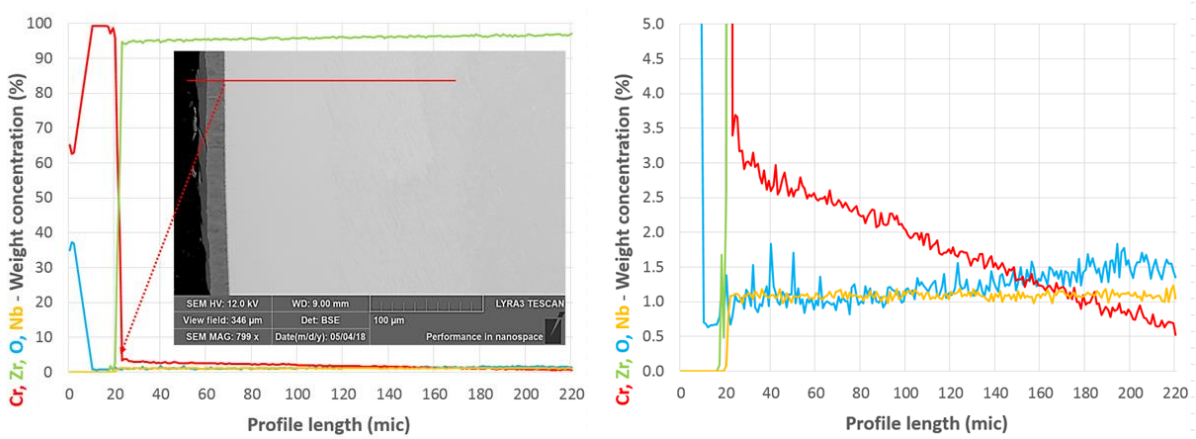

Fig. 11: Microstructure and position of WDS line-scan with O, Cr, Zr, Nb element concentration. Cr-coated sample after high-temperature steam oxidation at 1200°C, 30 minutes is shown.

Microhardness analysis in the prior β-Zr phase region (inner part and middle part of the single-sided oxidized sample) was performed in 2x10 positions. Measured values of HV0.1 in relation with RCT residual ductility at 135°C are shown in Fig. 12 (right). The results of inner-part row showed good agreement with DBT for uncoated M5 alloy [24]. The middle-row values were slightly higher. From the bulk oxygen content analysis, no oxygen gradient was observed, therefore, this difference can be explained due to Cr-diffusion and higher chromium content in the middle of the wall as studied by [25].

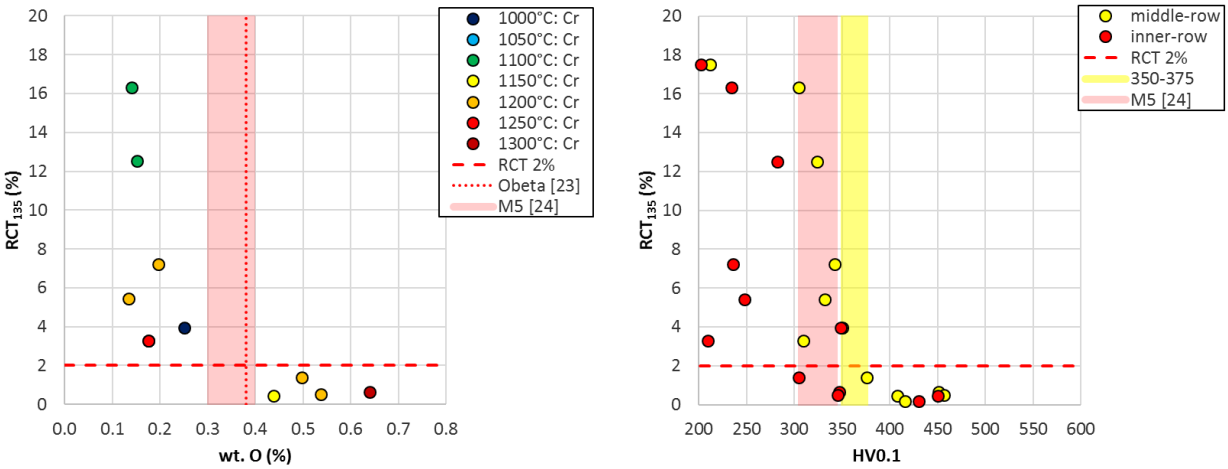

Fig. 12: Results of RCT residual ductility at 135 °C in relation with oxygen content (left) and microhardness (right). Comparison of Cr-coated specimens with limiting values for uncoated Zr-1%Nb alloys.

3.5 High-temperature Oxidation in Design Extension Conditions

Several experiments were done with coated samples at temperatures above Cr-Zr eutectic temperature (1333°C). Data comparing steam oxidation and argon annealing are discussed. Cr1-coated samples for double side oxidation were heated up to temperature 1400°C.

In the first test, argon environment was used and after reaching 1400°C the specimen was quenched. Cross-section metallography and chemical analysis (Cr, Zr), are shown in Fig. 13 (a) and (b). A thin melted area with a higher level of chromium (~14 %) was found under the coated surface of the sample only. A part of the cladding wall from the unaffected region was evaluated. It was found that layer about 50 – 100 μm from the surface melted. Preliminary results of the similar test were previously presented in [26].

The second sample was pre-oxidized in steam at temperature 800°C for about 12 minutes to prevent the over-heating. Afterward, the sample was directly moved into 1400°C temperature zone where it was oxidized. The sample was quenched at the end of 2 minutes exposure. Cross-section metallography and chemical analysis (Cr, Zr), are shown in Fig. 13 (c) and (d). The ZrO_2 and α-Zr(O) layers can be seen on both sides of the sample. The higher chromium content (~15 - 16 %) was found in the middle of the cladding wall only. It can be concluded, that oxygen diffusion shifted chromium into the regions corresponding to prior β-Zr phase (with lower oxygen content). This accelerated Cr interaction with Zr leads to more severe oxidation and melting in comparison with argon environment. It can be expected, that due to oxygen diffusion above the eutectic temperature, chromium will diffuse through the whole cladding wall. Measurements of the reaction layers thicknesses showed slightly higher ZrO_2 thickness on the outer side of the specimen. It suggests higher oxidation rate of coated surface in comparison with the un-coated surface at temperatures above the eutectic point.

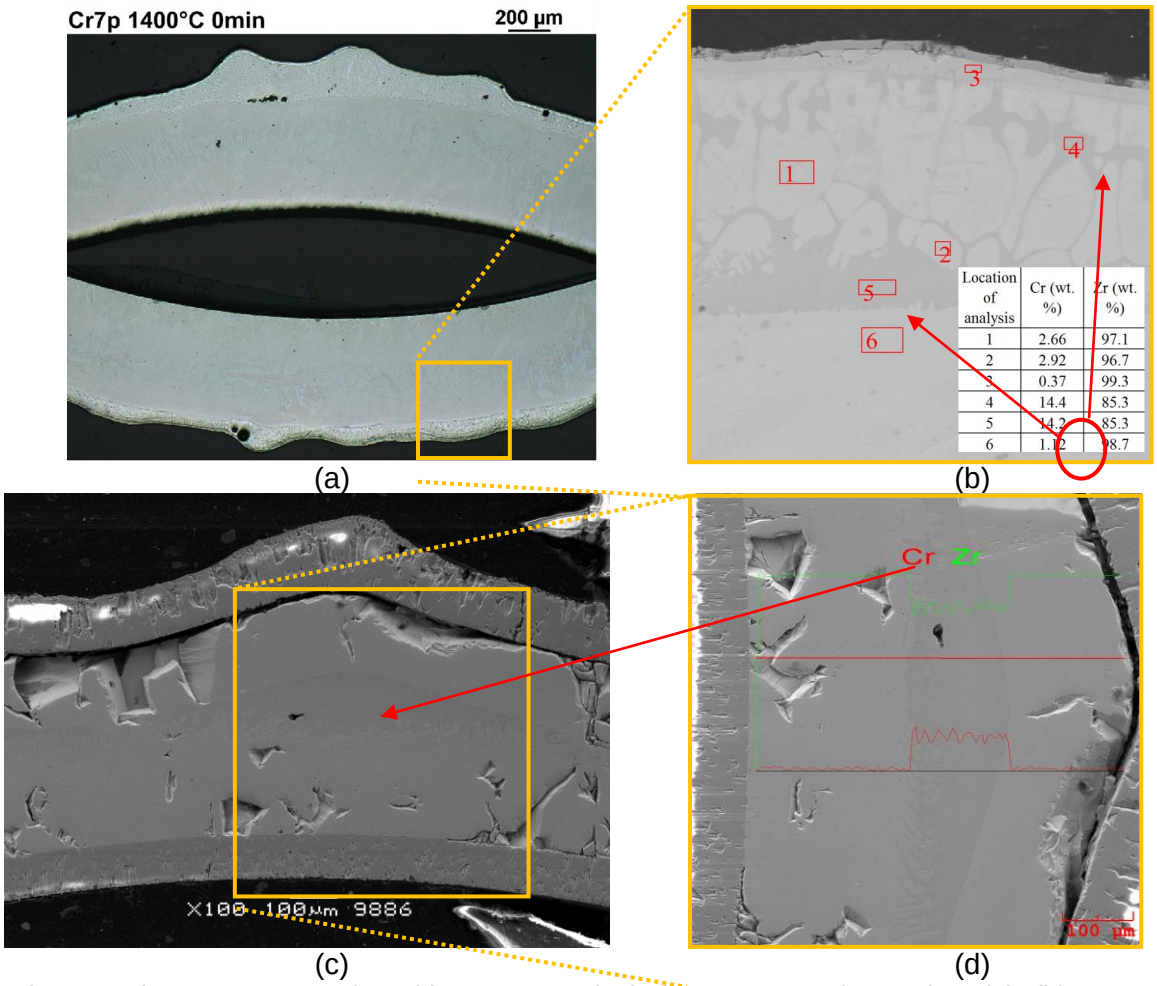

Fig. 13: Microstructure and position EDS analysis for Cr1-coated samples. (a), (b): 1400 °C / 0 min in argon environment (c), (d): 800 °C / 12 min + 1400 °C / 2 min in steam environment.

Similar experiments were performed with the other variants of chromium-based coatings: CrN (stoichiometric), $Cr_{90}N_{10}$ (sub-stoichiometric), and multi-layers: thin CrN+Cr (3 μm of CrN) and thick CrN+Cr (13 μm of CrN). Figure 14 shows the microstructure after the high-temperature oxidation in steam for $Cr_{90}N_{10}$-coating (a) and thin CrN+Cr-coating (b). Analysis showed, that in both cases the coating melted and oxidation from the outer coated side was slightly higher in comparison with the inner un-coated side.

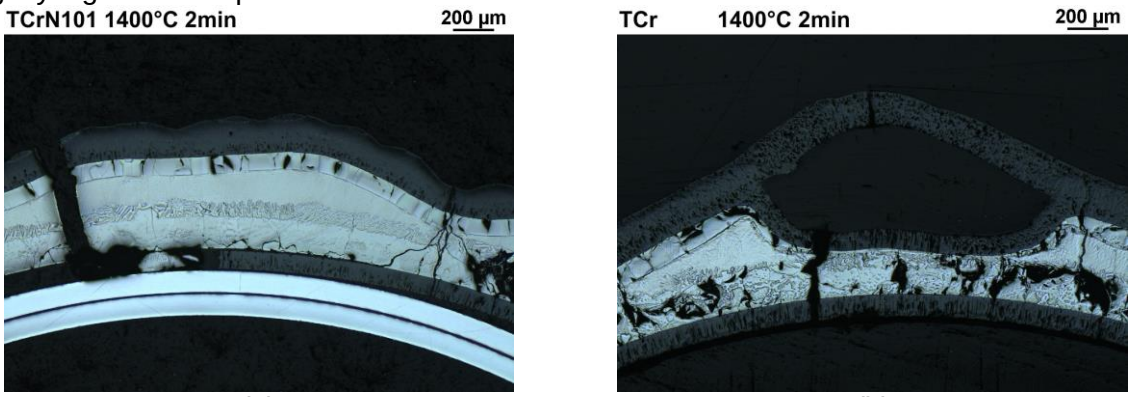

(a) (b)

Fig. 14: Microstructure of $Cr_{90}N_{10}$-coated (a) and thin CrN+Cr coated (b) specimens after high-temperature oxidation above the Cr-Zr melting temperature.

As was already published [25], CrN-coated specimens tested above eutectic point showed a resistance against melting at temperatures about 1400°C. On the other hand, the layers showed local failures of the coating due to CrN → Cr_2N + N_2 transformation and cracking during the temperature transient. An example of CrN coated sample after the high-temperature transient is shown in Fig. 15.

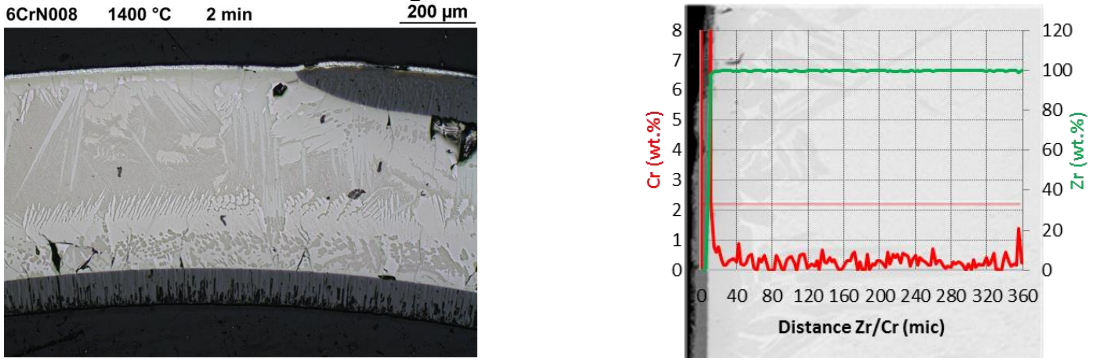

(a) (b)

Fig. 15: Microstructure of CrN-coated specimen after high-temperature oxidation above Cr-Zr melting temperature. (a) optical micrograph, (b) EDS line scan.

Presented experimental results of the double-sided oxidation with different layers inspired the authors to perform single-sided oxidation experiments with thick multi-layer CrN+Cr. The CrN underlying layer should be thick enough to produce sufficient amount of nitrogen during its phase transformation at high temperature which can then form a thin ZrN layer at the coating/substrate interface. It should be noted that CrN is stable up to about 800°C and the ZrN layer reducing the Cr diffusion and avoiding the eutectic formation will be present only in accidental conditions.

The experimental results of high-temperature oxidation at 1365°C are shown in Figure 16. No coating-substrate melting, coating spallation or local coating failures were observed (Fig. 17a). ZrN layer formed at the interface which prevents chromium diffusion into the Zr-alloy. Oxygen which diffused into the substrate formed α-Zr(O) layer and was localized below the coating (Fig. 17b). Two 7 mm wide rings were cut from specimen and RCTs at 135°C were performed (Fig. 17c). The RCT test was shut after 2 mm displacement and no cracks were observed, residual ductility was higher than 16 % (limiting value for DBT is considered as 2 %).

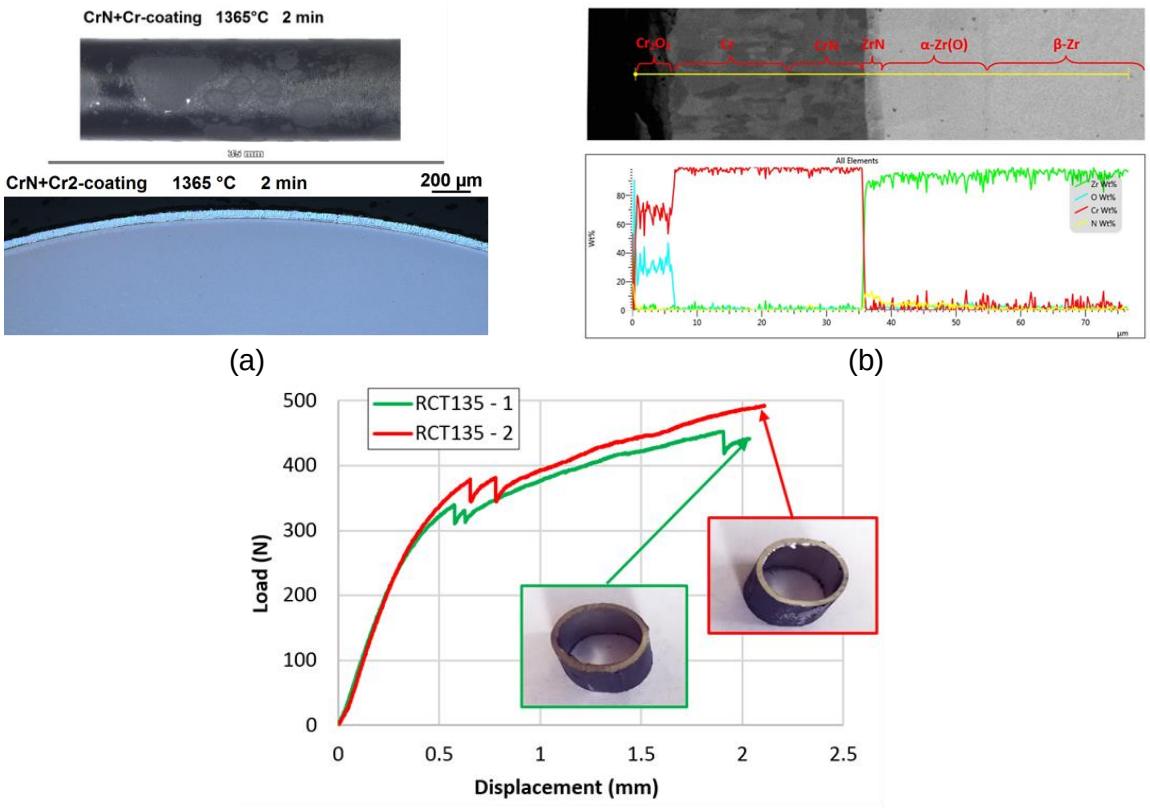

Fig. 16: Multi-layer "thick" CrN+Cr2-coated specimen after high temperature oxidation above Cr-Zr melting temperature. (a) Macrophotography (up) & optical micrograph (down), (b) EDS-line-scan at 5 kV acc. voltage, (c) RCT at 135 °C.

4 Discussion

High-temperature steam oxidation of Zirconium and Zirconium-based materials is an exothermal reaction. At high temperatures (over 1200°C), over-heating of cladding can occur. The sample temperature was measured by a thermocouple placed close to the surface. Therefore, it cannot be excluded that at the very beginning of the exposition the measured temperature was lower than the real surface temperature. However, declaring a higher oxidation rate for lower temperature is a conservative approach.

Observed cracking and local failures of CrN-coating at elevated temperatures are related to the phase transformation in microstructure (from CrN to Cr_2N + N_2). This decomposition occurs at temperatures below 850°C causing cracking of the coating due to density differences between CrN and Cr_2N. On the other hand, CrN-coating show very good results from the point of view of Cr-Zr eutectic formation and Cr-diffusion and consequent substrate embrittlement.

The main issues of pure Cr and stoichiometric CrN coatings during high-temperature oxidation were identified as: CrN-cracking, Cr-diffusion into the substrate and Cr-Zr melting. Therefore, authors performed tests with other variants of Cr-based coatings, namely: CrN-Cr multi-layer coating and substoichiometric CrN. For "thick" variant of CrN+Cr coating, ZrN-formation was observed, which probably enhances the resistance of claddings using Cr-based coatings during LOCA transient and especially at temperatures above Cr-Zr melting point.

The presented approach shows possibilities of improving PVD Cr-based coatings in the way of using CrN-Cr multi-layer coatings or non-stochiometric CrN coatings with gradient elements distribution that will be further studied in detail.

5 Conclusions

Long-term corrosion autoclave test was performed at the temperature of 360°C in the WWER water chemistry and the results up to 210 days are presented. The results show very low and stable weight gains and also drastically reduced hydrogen pickup. The characterization of as-

coated samples using EBSD, fracture analysis and XRD showed very strong orientation of coatings and the microstructural and phase changes between different types of deposited coatings also during the high-temperature transient. As was shown in previous studied, the burst tests for coated cladding showed a drastic reduction of displacement and decrease of the size of a balloon and burst which is valid also for the presented coatings.
The main part of the contribution is focused on the single-sided and double-sided high-temperature steam oxidation at temperatures between 1000 and 1400°C. The comparison between several types of Cr-based coatings was made (pure Cr, stoichiometric CrN, substoichiometric CrN and multilayer Cr+CrN). The high-temperature oxidation tests showed the protective behavior of coatings in the steam environment. RCT and microhardness measurements were performed after the high-temperature oxidation test. TEA method was used for bulk hydrogen and oxygen content measurements. Lathe machining was used to reduce wall thickness for measuring bulk-oxygen concentration in several rings from different cladding wall positions. Optical microscopy, scanning microscopy (EDS, WDS, EBSD), XRD were used for the evaluation of microstructure and chemical composition before and after the high-temperature oxidation tests. Based on the testing and characterization, three main issues entitled to pure Cr and stoichiometric CrN were identified – Cr enhanced embrittlement of Zr-based substrate, Cr-Zr eutectic formation and melting and CrN cracking.
Therefore, the paper proposes two possible ways of improving the PVD Cr-based coatings considered as perspective ATF cladding materials: Deposition of CrN-Cr multi-layer coatings and CrN-coatings with gradient elements distribution. These modifications can improve the behavior of claddings using the Cr-based coatings. When considering the multilayer Cr+CrN coating, the upper Cr-layer showed very good corrosion resistance and integrity. The CrN interlayer transforms to $Cr_2N + N_2$ which was observed during the high-temperature transient and confirmed by chemical analyses. The released nitrogen formed a thin stable ZrN layer, which prevents Cr-diffusion into the substrate and prevents the Cr-Zr melting due to eutectic formation at the temperature above 1350 °C as well.

Acknowledgments
The authors thank the whole UJP-zirconium department (namely: V. Rozkošný, J. Kočí, J. Šustr, D. Rada, P. Gajdoš, and V. Vrtílková) for sample preparation, running experiments, and post-experimental evaluation. Financial support of this research through ČEZ a.s. company is gratefully acknowledged. Also, this work was supported by the Ministry of Education, Youth and Sport of the Czech Republic, programme NPU1, project No LO1207, LO1402, National Programme of Sustainability II Project LQ1603 (Research for SUSEN), Grant Agency of the Czech Technical University in Prague, grant No. SGS16/252/OHK4/3T/14 and IAEA CRP 21065, Technology Agency of the Czech Republic grant No. TH02020477, CZ.2.16/3.1.00/21563, CZ.1.05/2.1.00/03.0088.

6 References

[1] S. J. Zinkle, K. A. Terrani, J. C. Gehin, L. J. Ott, and L. L. Snead, 'Accident tolerant fuels for LWRs: A perspective', *J. Nucl. Mater.*, vol. 448, no. 1–3, pp. 374–379, May 2014.
[2] K. A. Terrani, 'Accident tolerant fuel cladding development: Promise, status, and challenges', *J. Nucl. Mater.*, vol. 501, pp. 13–30, Apr. 2018.
[3] L. Braase, 'Enhanced Accident Tolerant LWR Fuels National Metrics Workshop Report', Idaho National Laboratory (INL), INL/EXT-13-28090, Jan. 2013.
[4] J.-H. Park, H.-G. Kim, J. Park, Y.-I. Jung, D.-J. Park, and Y.-H. Koo, 'High temperature steam-oxidation behavior of arc ion plated Cr coatings for accident tolerant fuel claddings', *Surf. Coat. Technol.*, vol. 280, pp. 256–259, Oct. 2015.
[5] C. Tang, M. Stueber, H. J. Seifert, and M. Steinbrueck, 'Protective coatings on zirconium-based alloys as accident-tolerant fuel (ATF) claddings', *Corros. Rev.*, vol. 35, no. 3, pp. 141–165, 2017.
[6] I. Younker and M. Fratoni, 'Neutronic evaluation of coating and cladding materials for accident tolerant fuels', *Prog. Nucl. Energy*, vol. 88, pp. 10–18, Apr. 2016.
[7] IAEA, 'Accident Tolerant Fuel Concepts for Light Water Reactors', 2016.

[8] H.-G. Kim, I.-H. Kim, Y.-I. Jung, D.-J. Park, J.-Y. Park, and Y.-H. Koo, ‘Adhesion property and high-temperature oxidation behavior of Cr-coated Zircaloy-4 cladding tube prepared by 3D laser coating’, *J. Nucl. Mater.*, vol. 465, pp. 531–539, Oct. 2015.
[9] A. S. Kuprin *et al.*, ‘Vacuum-arc chromium-based coatings for protection of zirconium alloys from the high-temperature oxidation in air’, *J. Nucl. Mater.*, vol. 465, pp. 400–406, Oct. 2015.
[10] M. Ševeček *et al.*, ‘Development of Cr Cold-Spray Coated Fuel Cladding with Enhanced Accident Tolerance’, *Nucl. Eng. Technol.*
[11] W. Zhong, P. A. Mouche, and B. J. Heuser, ‘Response of Cr and Cr-Al coatings on Zircaloy-2 to high temperature steam’, *J. Nucl. Mater.*, vol. 498, pp. 137–148, Jan. 2018.
[12] J. Brachet *et al.*, ‘Behavior under LOCA conditions of Enhanced Accident Tolerant Chromium Coated Zircaloy-4 Claddings’, *Top Fuel 2016 Boise ID Sept. 11-15 2016*, 2016.
[13] K. Daub, R. Van Nieuwenhove, and H. Nordin, ‘Investigation of the impact of coatings on corrosion and hydrogen uptake of Zircaloy-4’, *J. Nucl. Mater.*, vol. 467, pp. 260–270, Dec. 2015.
[14] J. Krejci, M. Sevecek, and L. Cvrcek, ‘Development of Chromium and Chromium Nitride Coated Cladding for VVER Reactors’, *2017 WRFPM*.
[15] R. Van Nieuwenhove, V. Andersson, J. Balak, and B. Oberländer, ‘In-Pile Testing of CrN, TiAlN, and AlCrN Coatings on Zircaloy Cladding in the Halden Reactor’, in *Zirconium in the Nuclear Industry: 18th International Symposium*, 2018.
[16] J. Rabe, K. Daub, H. Nordin, R. Van Nieuwenhove, T. Karlsen, Marie, and R. Szőke, ‘Investigation of PVD Coatings for Nuclear Applications: Hight Temperature Steam Exposure Testing’, *Nucl. Mater. Conf. NuMat 2016*, 2016.
[17] J. Krejčí, M. Ševeček, L. Cvrcek, J. Kabátová, and F. Manoch, ‘Chromium and Chromium Nitride Coated Cladding for Nuclear Reactor Fuel’, in *Proceedings of the 20th International Corrosion Congress, EUROCORR 2017*, Prague, Czech Republic, 2017.
[18] A. Krausová, L. Tůma, M. Novák, L. Cvrček, J. Krejčí, and J. Macák, ‘Chromium Coating as a Surface Protection of Zirconium Alloys’, *Koroze Ochr. Mater.*, vol. 61, no. 5, pp. 169–172, Dec. 2017.
[19] R. E. Pawel, J. V. Cathcart, and R. A. McKee, ‘The Kinetics of Oxidation of Zircaloy-4 in Steam at High Temperatures’, *J. Electrochem. Soc.*, vol. 126, no. 7, pp. 1105–1111, Jan. 1979.
[20] R. E. Williford, ‘Safety Margins in Zircaloy Oxidation and Embrittlement Criteria for Emergency Core Cooling System Acceptance’, *Nucl. Technol.*, vol. 74, no. 3, pp. 333–345, Sep. 1986.
[21] Y. Yan, B. E. Garrison, T. S. Smith, M. Howell, J. R. Keiser, and G. L. Bell, ‘Investigation of High-temperature Oxidation Kinetics and Residual Ductility of Oxidized Samples of Sponge-based E110 Alloy Cladding Tubes’, *MRS Adv.*, vol. 2, no. 21–22, pp. 1203–1208, 2017.
[22] C. GRANDJEAN and G. HACHE, ‘Cladding Oxidation. Resistance to Quench and Post-Quench Loads.’, p. 239.
[23] M. Négyesi *et al.*, ‘Proposal of new Oβ oxidation criterion for new types of the Zr1Nb alloy of fuel claddings’, *Nucl. Eng. Des.*, vol. 261, pp. 260–268, Aug. 2013.
[24] J. Brachet *et al.*, ‘Hydrogen Content, Preoxidation, and Cooling Scenario Effects on Post-Quench Microstructure and Mechanical Properties of Zircaloy-4 and M5® Alloys in LOCA Conditions’, *Zircon. Nucl. Ind. 15th Int. Symp.*, Jan. 2009.
[25] X. Wenxin and Y. Shihao, ‘Reaction diffusion in chromium-zircaloy-2 system’, China Nuclear Information Centre, CNIC--01562, 2001.
[26] J. Bischoff *et al.*, ‘AREVA NP’s enhanced accident-tolerant fuel developments: Focus on Cr-coated M5 cladding’, *Nucl. Eng. Technol.*, vol. 50, no. 2, pp. 223–228, Mar. 2018.